THE ASTROPHYSICAL JOURNAL, 483:731–744, 1997 July 10

ORBITS IN THE BAR OF NGC 4314

P. A. PATSIS,[1,2] E. ATHANASSOULA,[2] AND A. C. QUILLEN[2,3]
Received 1996 December 19; accepted 1997 February 10

ABSTRACT

We find the main families of simple periodic orbits in and around the bar of NGC 4314 and examine their stability. In many ways, our results agree with those found for model barred galaxies, yet our realistic potential allows us to go further in a comparison with the galaxy morphology. In particular, we underline the importance of the families of periodic orbits that are asymmetric with respect to the bar minor axis.

The x_1 family provides the building blocks for the bar. In the inner parts we find orbits that are roughly perpendicular to the bar, although their shape and orientation vary along the corresponding families. As in previous studies, we find a symmetric unstable 3:1 family, but we also find an asymmetric and stable 3:1 family. We also find asymmetric diamond-like orbits near corotation. We pay special attention to the orbital behavior at the ultraharmonic resonance region, and we investigate all possibilities offered by our study in explaining the boxy structure at the end of the bar.

Subject headings: galaxies: individual (NGC 4314) — galaxies: kinematics and dynamics — galaxies: structure

1. INTRODUCTION

The present paper is concerned with the orbital structure in the barred galaxy NGC 4314, which is classified as SBT1 by de Vaucouleurs et al. (1991). The evaluation of its potential from near-infrared observations by Quillen, Frogel, & González (1994, hereafter QFG) offers the opportunity for orbital calculations in an analytic model. This in turn allows the comparison of results concerning the orbital structure in this particular galaxy with that expected from generic models of barred potentials.

Computations of orbits in barred potentials have been described in the past in papers too numerous to mention here. The reader, however, may consult the review by Contopoulos & Grosbøl (1989), as well as the articles cited throughout this paper and the references therein. In these kinds of studies the calculation of the stability of the periodic orbits is crucial. Stable periodic orbits, which are followed by a large set of nonperiodic orbits, may account for the presence of particular morphological features in their neighborhood, since they provide the building blocks (Athanassoula et al. 1983) for the observed structures. The major aim of our work is to find the existing families of periodic orbits in the QFG potential and to estimate their importance for the observed morphology of NGC 4314.

Recent near-infrared observations of barred galaxies (Friedli et al. 1996; QFG; Quillen et al. 1995a, 1995b; Regan, Vogel, & Teuben 1995; Shaw et al. 1995) have shown that, at these wavelengths as well, nuclear bars, triaxial bulges, twisted isophotes, as well as boxy isophotes at the end of the main bar, are typical morphological features. Since cool giants and dwarfs are much better tracers of the mass distribution in a galaxy than the hotter stars (Frogel 1988), a potential based on near-infrared observations offers the most reliable estimate for the smoothed-out gravitational field in which the orbits of stars should be calculated. The intrinsic shape also is more accurately shown in the near-infrared because of the much smaller amount of extinction at those wavelengths (Block et al. 1994). One of our goals in this paper will be to find the connection between the orbits and the intrinsic shape of the galaxy.

Athanassoula et al. (1990), using a sample of 12 galaxies, showed that early-type, strongly barred galaxies have rectangular-like isophotes, particularly near the ends of the bar. NGC 4314 is one of the galaxies of the Athanassoula et al. (1990) sample for which this effect was the clearest. It is not, however, easy to find which orbits are responsible for this shape, since the rectangular orbits found in the ultraharmonic resonance (UHR) region initially by Athanassoula et al. (1983) (see also Pfenniger 1984a; Contopoulos 1988; Contopoulos & Grosbøl 1989) are not always stable in models representing barred galaxies like NGC 4314. This, together with alternative solutions including other types of orbits, was discussed by Athanassoula (1991, 1996). Such alternative solutions include quasi-periodic orbits wobbling around an x_1 orbit, superposition of two 3:1 orbits symmetric with respect to the bar major or minor axes, or ergodic orbits trapped by cantori, i.e., staying for relatively long times bound in parts of phase space inside chaotic regions. Since the QFG potential is the most appropriate one among the potentials used so far to study this problem, we will explicitly examine all these alternative solutions. In particular, in this paper we will not restrict ourselves to orbits starting perpendicular from the bar minor axis, as is done in many orbital studies, thus obtaining a more complete coverage of the families of periodic orbits.

Another way to study the orbital structure of barred galaxies is through N-body simulations. Comparisons of orbits taken straight from the self-gravitating simulations with those found in analytic potentials strengthen the conclusions about the type of orbits making the bar and those that contribute to the density in the outer disk (Sparke & Sellwood 1987; Pfenniger & Friedli 1991; Sundin 1993; Sundin et al. 1993; Kaufmann & Contopoulos 1996). Such a comparison is also among our motivations for carrying out the present work.

[1] Max-Planck-Institut für Astronomie, Königstuhl 17, D-69117 Heidelberg, Germany.
[2] Observatoire de Marseille, 2 Place Le Verrier, F-13248 Marseille, Cedex 4, France.
[3] Ohio State University, Department of Astronomy, 174 West 18th Avenue, Columbus, OH 43210.

In the next section we present the potential we use and our methods. In § 3 we discuss the axisymmetric model and in § 4 the orbital structure in a model having only the cosine terms of the QFG potential. The results for the complete model, with both sine and cosine terms, are given in § 5. Finally, our results are summarized and discussed in § 6.

2. POTENTIALS AND METHODS

2.1. *The Potentials*

The small inclination angle of NGC 4314 (estimated at 23° by Grosbøl 1985), its small bulge size (Benedict et al. 1992, 1993), and the constant near-infrared colors across its bar, which indicate a constant mass-to-light ratio (QFG), make it well suited for the evaluation of its potential from observations. QFG write the potential in the $z = 0$ plane as a Fourier series,

$$\Phi(r, \theta) = \Phi_0(r) + \sum_{m>0} [\Phi_{mc}(r) \cos m\theta + \Phi_{ms}(r) \sin m\theta] , \quad (1)$$

and the coefficients of the various components in the form $\sum_{n=0}^{8} \alpha_n r^n$. Using the K surface brightness of the galaxy and assuming a sech^2 law with a vertical scale height $h = 7''.4$ for the z distribution, they calculate the values of the $m = 0$, 2, 4, and 6 coefficients α_n (their numerical values can be found in $\mathrm{km}^2\ \mathrm{s}^{-2}$ in Table 1 of QFG). We will use this potential for our orbit calculations, keeping only the $m = 0$, 2, and 4 terms, since the $m = 6$ terms are of low amplitude and badly defined because of the noise (cf. Fig. 4 of QFG). Furthermore, in order to assess the importance of asymmetries, we will also calculate orbits in a potential including, besides the axisymmetric part, the $\cos 2\theta$ and $\cos 4\theta$ terms. We will call this latter model "model C" (C for cosine), while we will refer to the model with both the sine and the cosine terms as "model T" (T for total). In both cases the calculations for our standard models have been done in a frame rotating with $\Omega_b = 44.96$ km s^{-1} kpc^{-1}. This gives a corotation radius of 3.57 kpc, which roughly corresponds to 70″, as proposed by QFG. The bar is estimated to end at 60″, or 0.86 r_c, i.e., toward the middle of the range given by Athanassoula (1992a, 1992b) for early-type, strongly barred galaxies. The ratio Φ_{2c}/Φ_0 varies between 0 and 0.1, while the absolute value of the corresponding ratio for the sine terms is always less than 0.02. For the $m = 4$ term the maximum of Φ_{4c}/Φ_0 is ≈ 0.02, while the corresponding sine ratio varies roughly between 0 and -0.01. All the above describe the relative strength of the various components of the potential. The reader is referred to Table 1 and Figure 4 in QFG for more information.

2.2. *Calculation of Periodic Orbits and of Their Stability*

The equations of motion are derived from the Hamiltonian,

$$H \equiv \tfrac{1}{2}(\dot{x}^2 + \dot{y}^2) + \Phi(x, y) - \tfrac{1}{2}\Omega_b^2(x^2 + y^2) = E_J , \quad (2)$$

where (x, y) are the coordinates in a Cartesian frame of reference corotating with the bar with angular velocity Ω_b, $\Phi(x, y)$ is the potential in Cartesian coordinates, E_J is the numerical value of the Jacobian integral, and dots denote time derivatives. Throughout this paper E_J is given in (km s^{-1})^2. We use a fourth-order Runge-Kutta integration scheme with a variable step. We find the periodic orbits by using an iterative Newton method in two dimensions. The families whose members are symmetric with respect to the bar minor axis are best followed on an (E_J, x) diagram, known as the characteristic diagram. The characteristic of a family of periodic orbits on this diagram is a curve giving the initial position along the bar minor axis, x, as a function of the Jacobi constant E_J. Orbits that are symmetric with respect to the minor axis are uniquely defined on such a diagram. For asymmetric orbits one also needs the corresponding initial velocity ($\dot{x}$), and the characteristic diagram becomes three-dimensional $(E_J, x, \dot{x})$. In our study we give special emphasis to asymmetric orbits, since they have not been extensively studied in the past and their role has not been thoroughly examined. In most cases, however, we will continue discussing orbits in terms of their position on the (E_J, x) diagram for reasons of continuity with previous work. We will also use Poincaré surfaces of section for studying in one go the complete orbital behavior for a given value of the Jacobi constant.

The changes in the stability of a family of periodic orbits as one of the parameters of the model varies (usually the energy) are followed by means of the characteristic diagram and the variation of Hénon's stability index (Hénon 1965). According to Hénon's method, after a periodic orbit is found with initial conditions, e.g., $(x_0, \dot{x}_0)$, a nonperiodic orbit in its close neighborhood is integrated. Then one considers the initial $(\delta x_0, \delta \dot{x}_0)$ and final $(\delta x_1, \delta \dot{x}_1)$ deviations of the nonperiodic orbit from the initial conditions of the periodic one. This is done at two successive upward intersections of the nonperiodic orbit by the axis $y = 0$. This way a $\boldsymbol{g}$: $(\delta x_0, \delta \dot{x}_0) \rightarrow (\delta x_1, \delta \dot{x}_1)$ transformation is established, the Jacobian of which can be written as

$$J = \begin{pmatrix} a & b \\ c & d \end{pmatrix} ,$$

and the corresponding characteristic equation is $\lambda^2 - (a + d)\lambda + 1 = 0$. We used a deviation $\Delta = 10^{-6}$ from the periodic orbit to calculate the a, b, c, d values. Hénon's stability index α characterizes the stability of the periodic orbits and is defined as $\alpha = 1/2(a + d)$. The stability condition is the condition for having two complex conjugate roots of modulus 1 in the characteristic equation. An orbit is stable if $|\alpha| < 1$. The evolution of the stability of a family of periodic orbits as a function of the energy in the rotating frame is given in an (E_J, α) diagram. Of special interest in this diagram is the case when α becomes equal to 1 either by being tangent to or by intersecting the $\alpha = 1$ line, usually called the $\alpha = 1$ axis (see, e.g., Contopoulos & Grosbøl 1986). At these points, a new family is bifurcated and introduced into the system. It has the same periodicity as the parent family and inherits its stability. Thus, after a S → U transition, i.e., when a stable family becomes unstable, a new *stable* family is introduced into the system, and after a U → S transition, a new *unstable* one is introduced. Nevertheless, beyond their bifurcation point, the new bifurcated families may change their stability (Contopoulos & Grosbøl 1989). These changes of stability of the main, as well as of the bifurcated, families will be described in this paper by means of the characteristic and stability diagrams.

3. THE AXISYMMETRIC CASE

In the axisymmetric case one can always find the direct orbits, which are circular and which make up the "central"

[4] For the adopted distance $D = 10$ Mpc, this corresponds to 350 pc.

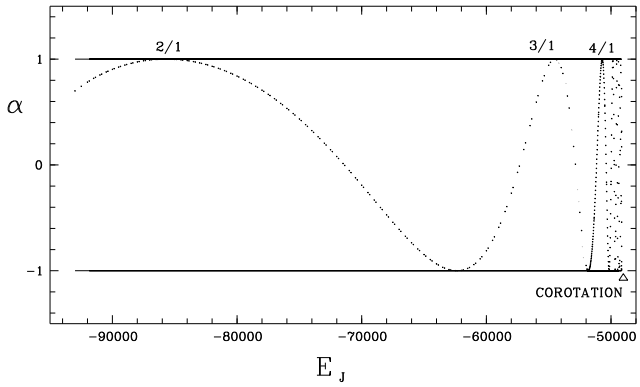

FIG. 1.—The stability index α as a function of E_J in the axisymmetric case. Three of the main resonances and corotation are marked.

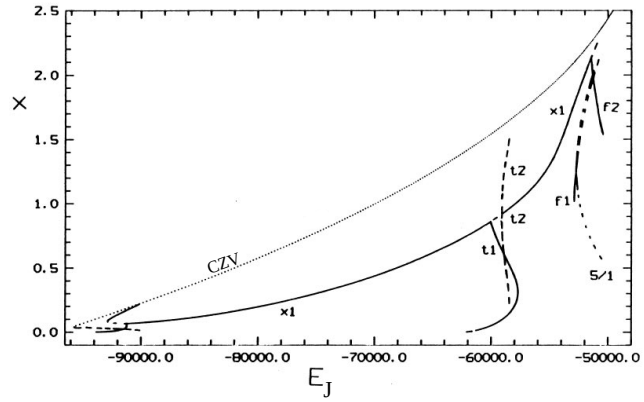

FIG. 2.—Characteristics of the main families of periodic orbits for model "C." The second branch of the bifurcating asymmetric families does not appear on this diagram. Unstable parts of the characteristics are given with dashed lines, while the curve of zero velocity is the dotted line labeled "CZV."

family, namely, the family that in general contains the ellipsoidal orbits that support the bar when the perturbation is added (see Contopoulos 1983a; see also the remark on p. 338 in Athanassoula 1992a). The characteristic of this family is a continuous line reaching the curve of zero velocity (CZV) at corotation. The variation of the stability index for the central family is presented in Figure 1 and shows that this family is stable everywhere. The stability curve oscillates between the limits of stability $|\alpha| = 1$ and reaches the $\alpha = 1$ axis at the resonances 2:1, 3:1, 4:1, and so on. The first three n:1 resonances are marked, as well as corotation. They appear in energies corresponding to distances of 0.28 kpc (2:1), 1.91 kpc (3:1), and 2.54 kpc (4:1). These, however, are the resonance distances in the axisymmetric case only. In the description of the nonaxisymmetric models we will see how the resonance distances are displaced with respect to those shown in Figure 1. The points beyond the 4:1 resonance are due to the successive ups and downs of the stability curve between $-1 < \alpha < 1$, in always shorter energy intervals as we approach corotation. In the axisymmetric case the radial distance between the 4:1 resonance and corotation corresponds to 1 kpc.

4. MODEL "C"

Model "C" consists of the axisymmetric and the cos 2θ and 4θ terms of the potential given in equation (1). We have calculated orbits in this potential in order to find the differences introduced by the presence of sine terms. This is particularly important since the sine terms are usually not included in general barred potentials used for orbital studies (for a review, see Contopoulos & Grosbøl 1989).

The main family in this model is the family of the elliptical-like orbits elongated along the bar and starting perpendicular from the bar minor axis, usually denoted by x_1 (Contopoulos & Papayannopoulos 1980). Its characteristic, as well as the characteristic of all other families playing a role in the dynamics of the system, is given in Figure 2. There are three areas of particular interest on this diagram. The area of the 2:1 and 1:1 resonances in the lower left-hand corner of Figure 2; the area of the 3:1 resonance around $E_J = -60{,}000$, where the families t_1 and t_2 are bifurcated; and finally the area beyond the 4:1 resonance, where the characteristic of x_1 has a gap and the families f_1, f_2, and 5:1 appear. The stability diagram of model "C" is given in Figure 3.

4.1. *Orbital Behavior Close to the Center*

Following the evolution of the x_1 characteristic toward lower energies, we observe that around $E_J = -93{,}000$, the curve bends upward to the right and ends on the CZV. For lower x in the same region, another branch appears, so that a gap is formed. The part of Figure 2 corresponding to $-96{,}000 < E_J < -86{,}400$ is given in enlargement in Figure 4. We note that the QFG potential is not realistic in the center. However, we did not observe any strange mathematical behavior due to this. In any case, the potential used

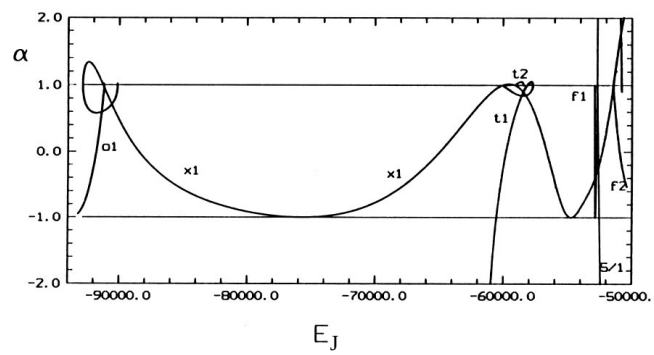

FIG. 3.—The stability curve of x_1 and its bifurcations for model "C"

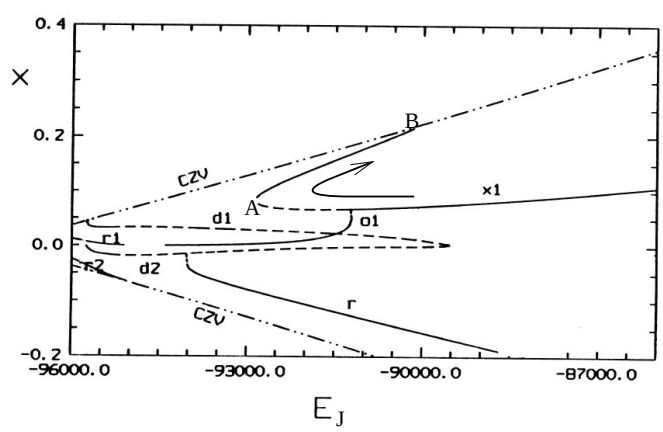

FIG. 4.—The evolution of the characteristic of x_1 close to the region of the 2:1 and 1:1 resonances for model "C."

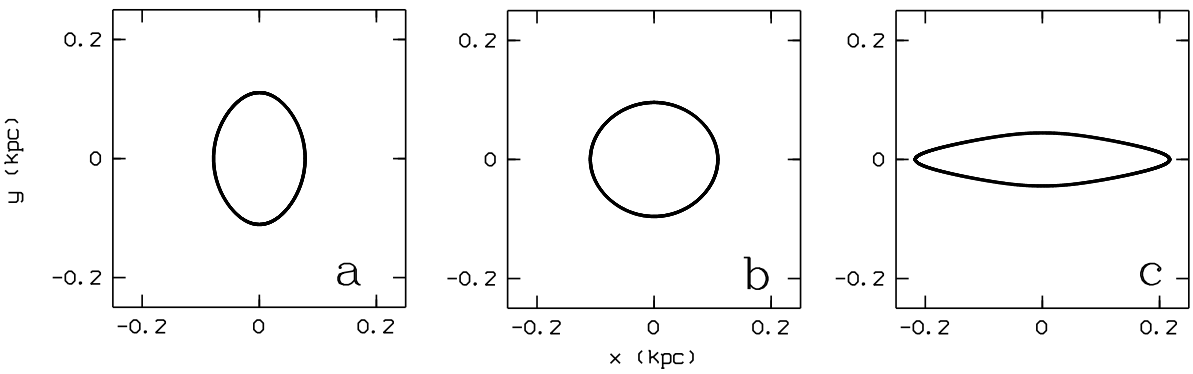

FIG. 5.—The evolution of the morphology of periodic orbits belonging to the family x_1 as we move on its characteristic in the direction of the arrow in the previous figure. In (*a*) we have an orbit at the right of A ($E_J = -92{,}846$), while in (*b*) and (*c*) we have two orbits from the part of the characteristic between A and B ($E_J = -92{,}544$ and $E_J = -90{,}156$, respectively).

for our calculations is not representative of the potential of NGC 4314 for distances smaller than 20″ (1 kpc), where a bulge component exists (QFG) and where the assumption of a constant thickness is not appropriate. Nevertheless, we examined the orbital morphology and stability in this region for completeness' sake. Figure 4 refers to radii <300 pc, i.e., the area where a nuclear ring is observed in NGC 4314 (Garcia-Baretto et al. 1991). The shape of the x_1 orbits is, as usual, elliptical. However, moving on the x_1 characteristic in the sense of the arrow in Figure 4, the eccentricity of the orbits decreases, and, finally, for orbits between points A and B, the minor axis of the ellipses is along the *y*-axis of the bar. This way the orientation of the stable elliptical orbits changes, providing the system with stable orbits such as, in other systems, those of the families x_2 and x_3 (Contopoulos & Papayannopoulos 1980; Athanassoula 1992a, 1992b). This evolution of the form of the orbits in this region can be seen in Figure 5.

In Figure 4, as well as in subsequent (E_J, x) diagrams, the unstable parts of the characteristic curves are given with dashed lines. We can thus see that the x_1 family has an unstable part close to point A. Moving to larger E_J, a U → S transition occurs near $E_J = -91{,}500$. There, family o_1 is bifurcated. Initially, this family is unstable, but it soon becomes stable and turns toward lower energies. The topology of the stable orbits of the o_1 family changes in an interesting way as we move to the left in Figure 4. This is shown in Figure 6, starting from orbit "1," which is the orbit exactly at the bifurcating point, and going to orbit "5." The first orbits are ellipses inclined with respect to the bar minor axis. For even lower energies they fold, giving stable orbits like those labeled by "4" and "5." The extent of these orbits is less than 200 pc. We note that we find two branches of family o_1. They have the same initial x values but different $\dot{x}$. So in the (E_J, x) diagram in Figure 4, both branches are represented by the same curve.

Other families of periodic orbits found close to the center are the two branches of family *d*, labeled in Figure 4 by d_1 and d_2; the retrograde family *r*; and finally two more branches of a family denoted by r_1 and r_2. Families d_1 and d_2 are unstable over the major part of their energy range and have only small stable parts very close to the center. When stable, they are very small and "bean shaped," and the orbits of each branch have always positive, or, respectively, always negative, x values. The unstable (Fig. 7) orbits of this family resemble the 1:1 orbits found by

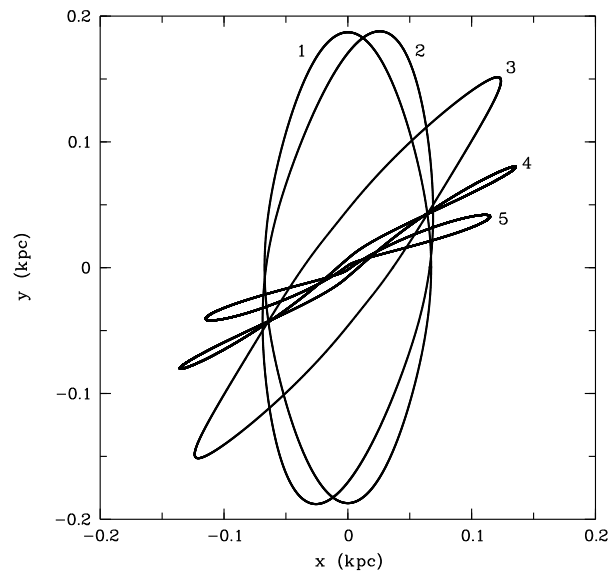

FIG. 6.—Stable orbits belonging to family o_1. Along the sequence 1 to 5 we move from larger to smaller energies.

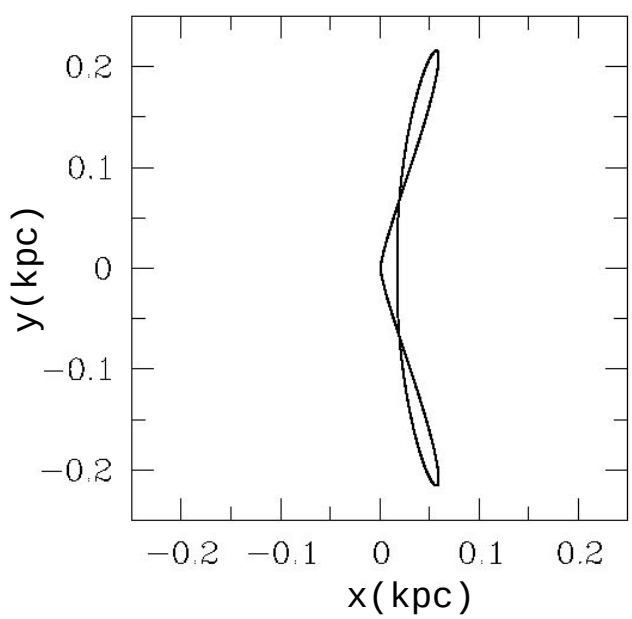

FIG. 7.—A typical unstable *d* orbit

Papayannopoulos & Petrou (1983). Families r_1 and r_2 have shapes similar to d_1 and d_2 but are described in the opposite sense. All orbits mentioned in this paragraph seem to play a minor role, even in the local dynamics of the system.

4.2. *The 3:1 Resonance Region*

As shown in Figure 3, family x_1 has a small unstable part close to $E_J = -60{,}000$, where $\alpha > 1$. This implies a S → U and a U → S transition, which will bring two new simple periodic families into the system, which we will call, respectively, t_1 and t_2. The t_1 orbits have a triangular shape with one side roughly parallel to the bar minor axis and have been missed in many surveys since they do not start off perpendicular from the x-axis. As shown in Figure 8, there are two t_1 branches, symmetric with respect to the bar minor axis. Two corresponding orbits of the two families have initial $\dot{x}$ values of opposite signs and the same x and E_J values. Thus they share the same location on the (E_J, x) diagram. Away from the bifurcating point they develop loops at the "corners" of the triangles, the largest loop being along the bar major axis. The maximum extent of orbits belonging to this family along the major axis of the bar is almost 2.5 kpc. The family t_2 consists of unstable 3:1 orbits symmetric with respect to the bar minor axis, found in many other models (see, e.g., Athanassoula 1992a, 1992b). An example is given in Figure 9, and its branches—above and below the x_1 characteristic—are given in Figure 4. As in other models, the families of orbits generated at the 3:1 resonance affect the dynamics of the system only locally, since they have stable parts only at this region.

4.3. *Orbits around the UHR Resonance*

In this section we will discuss the stability of periodic orbits around the UHR and their possible connection with the rectangular-like isophotes around the end of the bar in NGC 4314.

The appearance of gaps in the characteristics around the UHR region and the coexistence of two families beyond it are typical of the orbital behavior in several bar potentials. These gaps are of two kinds. Either the original characteristic of family x_1 deviates upward and the "new" 4:1 family is found for the same E_J at smaller x values (type 1 gap), or the x_1 characteristic reaches a maximum x and then decreases. In this latter case the new branch can be found for the same E_J at larger x (type 2 gap) (Contopoulos 1988; Contopoulos & Grosbøl 1989). In both types the 4:1 family has a minimum E_J at the gap. In the first type the upper part of its characteristic curve is stable, while the lower is unstable. In the second type the upper part is unstable and the lower stable (see Fig. 1 in Contopoulos & Grosbøl 1989). Along the stable parts we may have transitions to instability and bifurcations of new families.

In Figures 10 and 11, respectively, we give close-ups of the characteristics of the main families and their stability curves close to the UHR for model "C." Figure 10 clearly

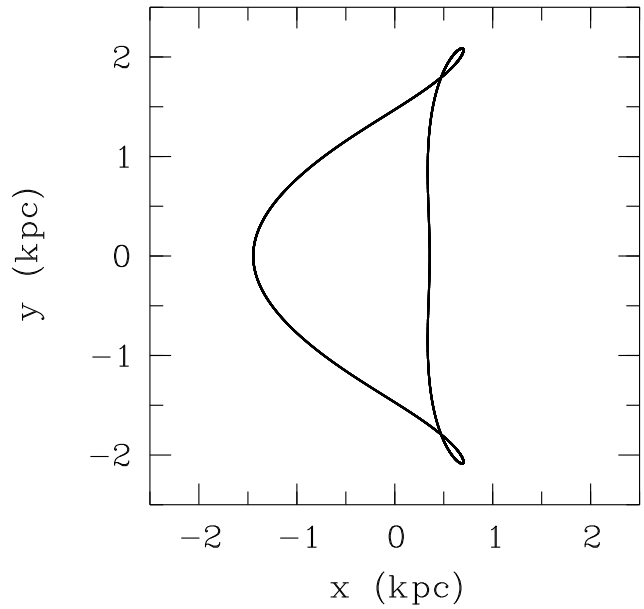

FIG. 9.—A typical symmetric 3:1 orbit belonging to the family t_2

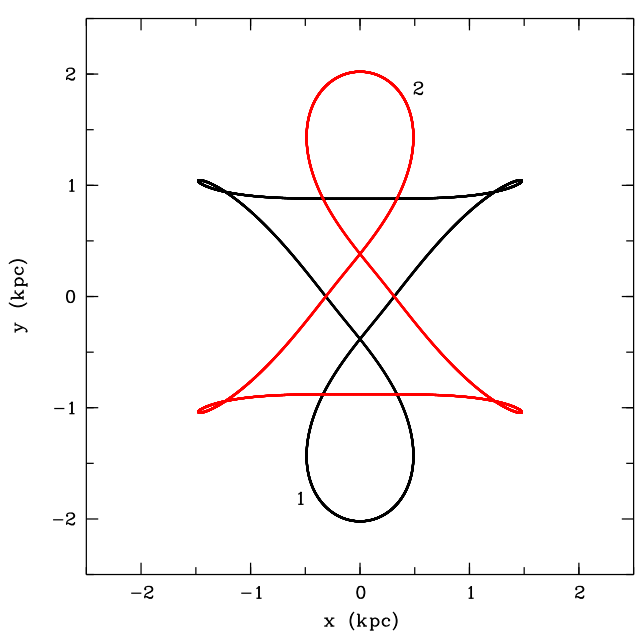

FIG. 8.—Two orbits of the t_1 family. They have the same position on the (E_J, x) diagram but belong to two different branches. The orbit labeled "1" has positive initial $\dot{x}$, while the orbit labeled "2" has negative initial $\dot{x}$.

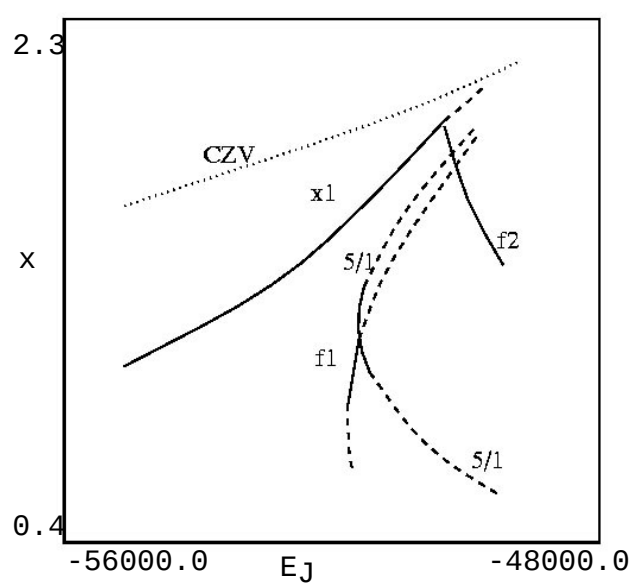

FIG. 10.—The characteristics of the main families at the UHR region of model "C."

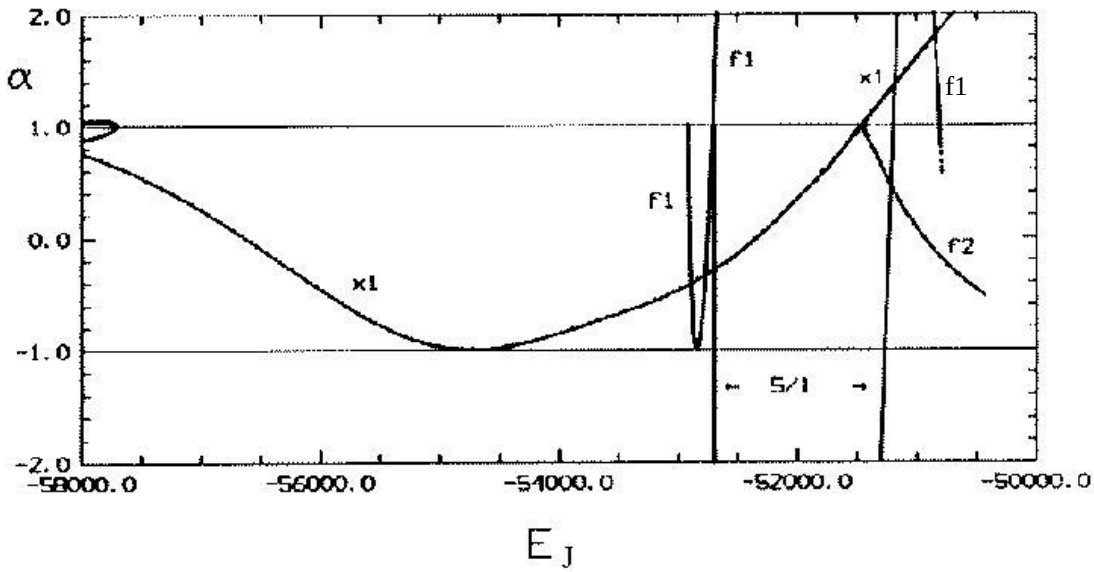

FIG. 11.—The stability curves of the main families at the UHR region of model "C"

shows that we are dealing with a hybrid kind of gap, which shares features of both types. Moving to the right toward corotation, first we encounter a gap that we can identify as "type 1," since the characteristic of x_1 deviates upward and the corresponding orbits are diamond-like and stable. A family f_1 coexists below the characteristic of x_1 and from it bifurcates at somewhat larger energies a 5:1 family, one branch of which remains very close to f_1. The situation locally closely resembles characteristics at the UHR region of a potential studied by Contopoulos (1983b), consisting of an isochrone axisymmetric part and a Barbanis & Woltjer (1967) bar perturbation. However, for slightly larger energies (at $E_J \approx -51{,}000$) x_1 becomes unstable, bifurcating another stable family (f_2). If one follows the evolution of the "stable path" first along the x_1 characteristic and then the f_1 family, one notices a behavior resembling that of a "type 2" gap, since this "stable path" presents a maximum x value. Yet, contrary to the "type 2" case, the orbits of the downward branch are diamond-like. The stable parts of the f_1 and 5:1 families are small, as can be estimated from Figure 11. In Figure 12 we give typical stable orbits of all families encountered at the UHR region of model "C."

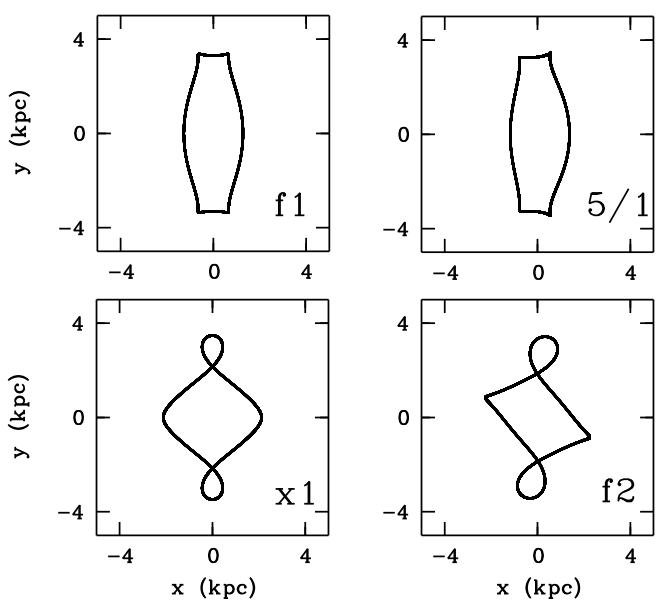

FIG. 12.—Stable orbits at the UHR region of model "C." In each box we include the name of the family to which the orbit belongs.

5. MODEL "T"

Model "C" has been used as an approximation of the total potential calculated by QFG for NGC 4314. In this section we will calculate the orbital structure in the total potential "T" and, by comparison, find the effect of the sine terms.

In this model even the x_1 orbits do not start perpendicular to the bar minor axis, thus even these orbits are not uniquely specified by their position in the (E_J, x) diagram. The interconnections of the several families of periodic orbits are more efficiently followed by means of their stability curves, given in Figure 13. For comparison with model "C," however, we give in Figure 14 the (E_J, x) projection of the (E_J, x, $\dot{x}$) diagram. For the 3:1 orbits, which are difficult to follow on the (E_J, x) diagram, we will give the full three-dimensional characteristics. In Figure 14 we include only one branch of each bifurcating family for simplicity. We see that close to the center the x_1 family evolves more smoothly than in model "C." At the 3:1 resonance it bifurcates two families of 3:1 periodic orbits, as did model "C," and finally

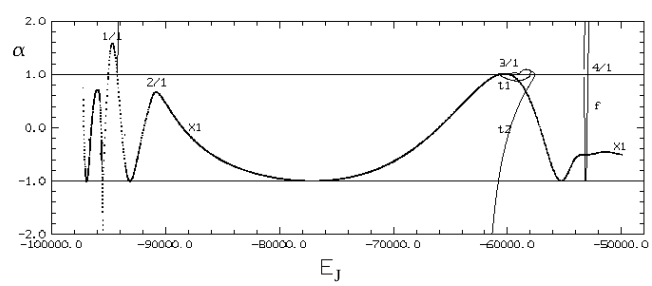

FIG. 13.—The stability diagram for family x_1 and for the bifurcating families in model "T."

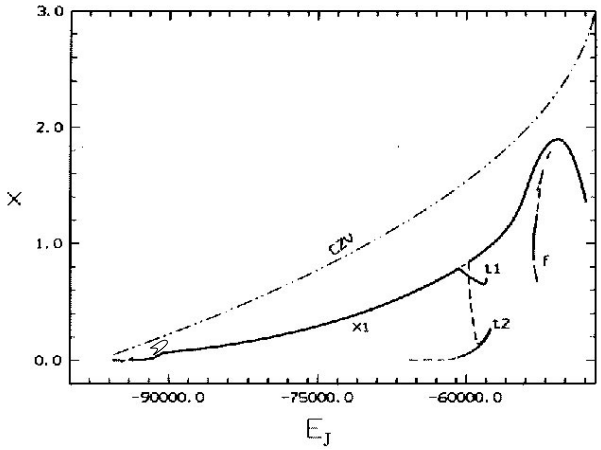

FIG. 14.—The (E_J, x) diagram displaying the main families of periodic orbits in model "T." Only one branch of each bifurcated family is included.

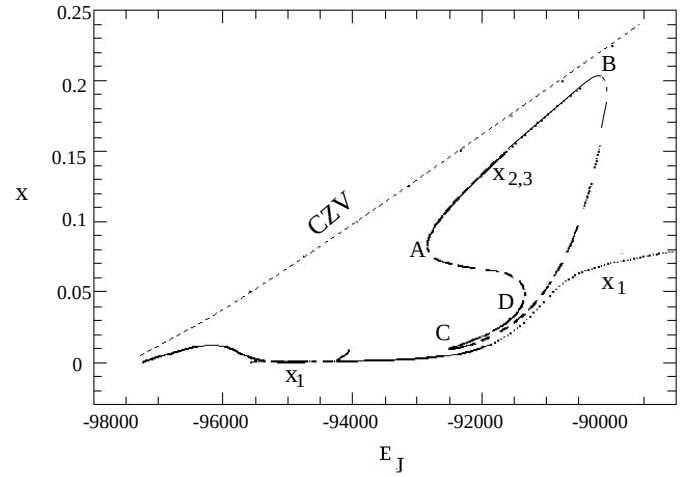

FIG. 16.—A closeup of the 2:1 and 1:1 resonance region in the (E_J, x) diagram of model "T." Unstable parts are denoted with dashed lines.

has a declining part just beyond the 4:1 resonance. Its stability curve levels off at the 4:1 resonance, thus showing the typical behavior of the stability index in this region (Contopoulos & Grosbøl 1986; Contopoulos & Grosbøl 1989). Let us now examine in more detail the various regions of interest.

5.1. *Orbits Close to the Center*

Moving from larger to smaller energies on the (E_J, x) diagram, we observe close to the center, at $E_J \approx -90{,}000$, a rather abrupt "drop" of the x_1 characteristic to even lower x values. Beyond this point the x_1 orbits get more and more inclined with respect to the major axis of the bar and, before falling onto the minor axis, develop loops. The evolution of their shapes follows that of the o_1 family in model "C" (Fig. 15). For the same E_J values and for larger x's we have another family of stable elliptical orbits, family $x_{2,3}$, whose characteristic forms a closed loop in the (E_J, x) plane. We have named it $x_{2,3}$ because of the location of its characteristic on the (E_J, x) plane and because the most elongated of its members are roughly aligned with the bar minor axis. Its orbits correspond to the orbits found in the up-going branch of the x_1 characteristic (between points A and B in Fig. 4) of model "C" and could be related to the observed nuclear ring located at this region of the galaxy, although this cannot be claimed with certainty since the QFG potential is inaccurate so close to the center. A blowup of the lower left-hand corner of Figure 14 is given in Figure 16. Family $x_{2,3}$ has two stable parts. One close to the CZV, and another close to x_1. Successive stable orbits along the upper stable part (AB) are given in Figure 17. The stable orbits at the lower stable part (CD) resemble the neighboring x_1 orbits but have inclinations of opposite sign.

Even closer to the center, at the 1:1 resonance, x_1 has a small unstable part. The bifurcating families there have shapes like orbit "3" in Figure 15, with one of the loops larger than the other. Finally for $E_J < -95{,}500$, we found a family of stable orbits orbiting around the center of the system having radii of a few pc. Let us again note that the

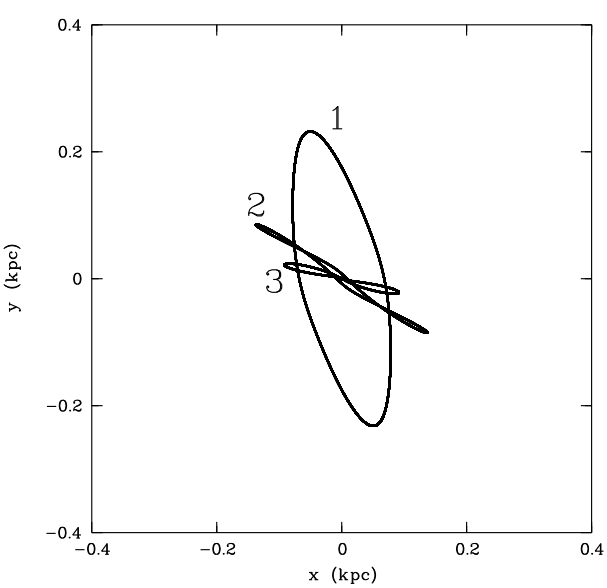

FIG. 15.—Close to the center the shape of the orbits of the x_1 family of model "T" have an evolution similar to that of the orbits of family o_1 in model "C." From 1 to 3 we move from larger to smaller E_J values.

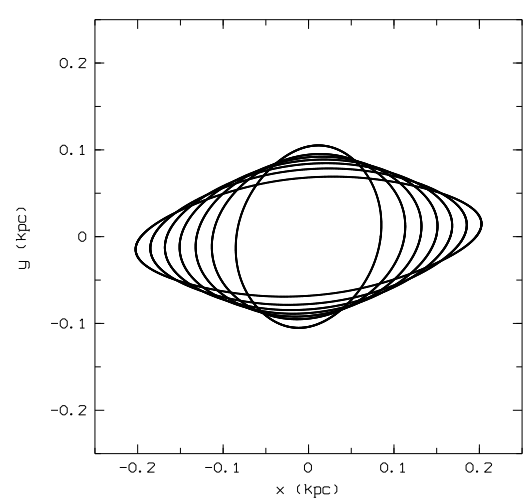

FIG. 17.—Successive stable orbits of the $x_{2,3}$ family. Orbits that are rounder and less inclined with respect to the bar minor axis orbits correspond to lower E_J values.

families appearing at the 2:1 and 1:1 resonances affect the dynamics of the system only locally.

5.2. *Orbits at the 3:1 Resonance*

As already mentioned, only one branch of each 3:1 family is plotted in Figure 14. The complete (E_J, x, $\dot{x}$) diagram around the 3:1 resonance is given in Figure 18. The curves wind in the three-dimensional space, and one has to rotate the figure in order to trace their exact shape. The bifurcated families change their initial stability away from the bifurcating point (Fig. 13). The shapes of orbits close to this point are as shown in Figures 19*a* and 19*c* for families t_1 and t_2, respectively. Their shapes, however, change as we move along the characteristic of each family. Family t_1 has triangular stable orbits (Fig. 19*b*) of the same kind as in model "C," but now completely asymmetric. The evolution of t_2 as we recede from the bifurcation point is also shown in Figure 19. It evolves along the sequence c → d → e → f while also changing its stability, and we observe that the orbits in the stable part have, like the orbits of family t_1, a triangular shape with a loop close to the major axis of the bar. Both our "C" and "T" models show a preference for loop structures along the major axis of the bar in this area. If one considers the two branches of family t_1 in both models, or the stable orbits of the t_2 family in model "T," then one gets figures with loops on both sides of the bar, similar to what we see in Figure 8. The role of the asymmetric orbits at the 3:1 resonance region, as well as at the UHR region that we will describe below, has, for comparison, also been investigated in the Ferrer's bar model used by Athanassoula (1992a, 1992b). We found good agreement between our results for the "C" and "T" models and those for this general model. This indicates that the stellar response at the 3:1 resonance found in the QFG potential is representative of a larger class of barred potentials.

5.3. *Simple Periodic Orbits at the UHR Resonance*

The stability index of x_1 levels off at the 4:1 resonance. This is a typical behavior found in several two-dimensional, and recently (Patsis & Grosbøl 1996) also in three-dimensional, galactic models. The leveling off seems to prevent family x_1 from bifurcating a new family, as it does in model "C." On the characteristic diagram (Fig. 14), the

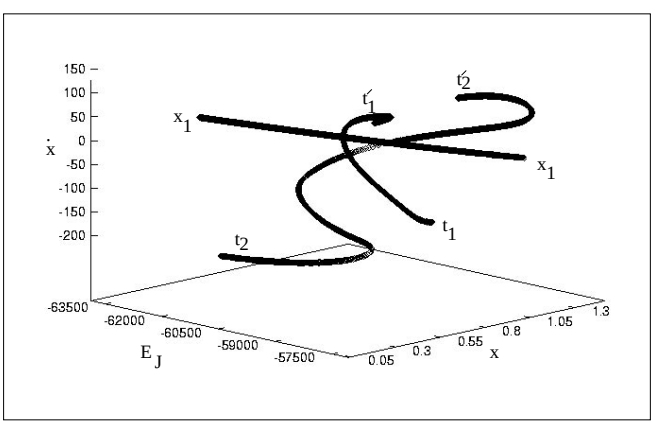

FIG. 18.—The characteristics of the main families at the 3:1 region of model "T." Considering the (E_J, x) plane initially being on the plane of the paper (E_J the horizontal axis and x the vertical one) and the $\dot{x}$ axis perpendicular to it, we have rotated the (E_J, x) plane 70° around the E_J axis and 45° around the $\dot{x}$ axis clockwise.

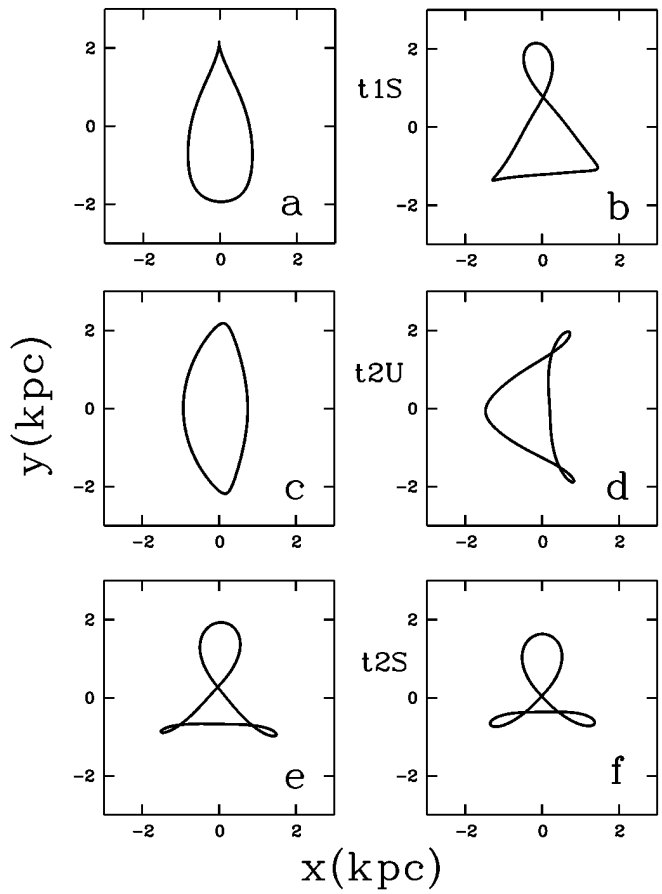

FIG. 19.—Orbits belonging to the 3:1 families t_1 and t_2 in model "T." (*a*) and (*b*) give two stable *t*1 orbits corresponding to $E_J = -60{,}485$ and $-58{,}024$, respectively, i.e., for values of E_J at the beginning and the end of the range for which the family exists. The orbits of t_2 are in a sequence of increasing distance along the characteristic of this family from the bifurcating point. They correspond to $E_J = -59{,}783$, $-59{,}073$, $-60{,}730$, and $-60{,}780$ for (*c*), (*d*), (*e*), and (*f*), respectively. All orbits are chosen from the branches depicted in Fig. 14.

curve of family x_1 reaches a maximum x and then decreases. One would thus expect a "type 2" 4:1 resonance gap in this case. The problem, however, is severely complicated by the presence of family *f*, at slightly lower energies. Close to its branching from the x_1, *f* bifurcates a 5:1 family. The range of stability of both these families is about the same as found in "C." Family *f*, as well as the 5:1 family in its stable part, are of rectangular-like shape. For the same energies the orbits of x_1 are diamonds having developed small loops. Thus the orbital behavior around UHR is quite different from the standard "type 2" case, where the part of the characteristic where x decreases with energy gives stable rectangular-like orbits. In our case we have in this region stable diamond-like orbits, corresponding to those found in family f_2 of model "C." The diamond-shaped orbits start being obviously inclined (i.e., they have large initial $\dot{x}$ values) with increasing E_J and for somewhat larger energies develop loops roughly along the minor axis of the bar. Let us now consider the relative extent of all these stable orbits at the UHR region. In general, the stable rectangular 4:1 orbits reach larger distances along the major axis of the bar than the corresponding x_1 orbits for the same E_J. Only for $-52{,}000 < E_J < -51{,}000$ the projections of the diamond-shaped x_1 orbits on the y-axis, i.e., along the bar major axis,

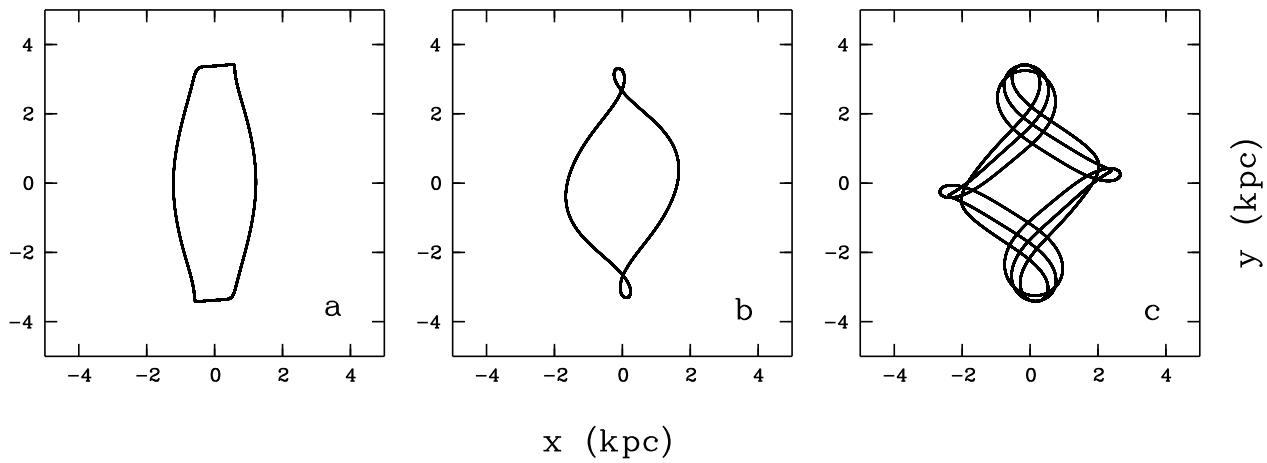

FIG. 20.—Stable orbits at the UHR region of model "T." In (*a*) we observe a typical *f* orbit, in (*b*) a diamond shaped x_1 orbit, and in (*c*) we observe how the orbits of this latter family evolve along the declining branch. Larger loops correspond to larger E_J values. The orbits in (*c*) do not help the bar to extend to larger distances along the major axis of the bar.

are as long as the projections of the rectangular-like orbits on the same axis. Beyond this point, i.e., for energies larger than roughly $E_J = -51{,}000$, the x_1 orbits become less elongated along the *y*-axis, with larger projections on the *x*-axis. As a result, the longest stable orbits along the bar major axis are found at the 4:1 resonance region. Shapes of stable periodic orbits and their relative positions are given in Figure 20.

5.4. *Other Orbits at the UHR Resonance*

We have also studied periodic orbits of multiplicity higher than 1, quasi-periodic and chaotic orbits in the UHR region. We looked at energies where both *f* and x_1 are stable, as well as at energies where the only stable family is x_1. A Poincaré cross section at $E_J = -53{,}248.175$ is given in Figure 21. The positions of the initial conditions of the orbits belonging to *f* and x_1 are marked by arrows. The space occupied by the invariants belonging to the *f* orbit is very small. An enlargement is given on the right-hand side of the figure. The larger stability regions observed in Figure 21 belong to stable periodic orbits of higher multiplicity. The most important are a double periodic orbit (marked with "db") and a triple periodic one (marked with "tr"). Their shapes are given in Figure 22. The double periodic orbit db is like a hybrid of the two 4:1 simple periodic orbits, while the triple one resembles figures combining the two branches of 3:1 stable orbits. Such triple orbits, like in the 3:1 families, have some "horizontal" segments. These segments are nearer to the center than the corresponding segments of the 4:1 rectangular-like orbits. By trying several randomly chosen initial conditions (always for the same E_J as in the Poincaré cross section) and integrating for times equal to about 10 orbital periods of the corresponding periodic orbits, it becomes clear that the motion of the test particles is reminiscent of both kinds of stable simple periodic orbits existing in the system. In most of the cases

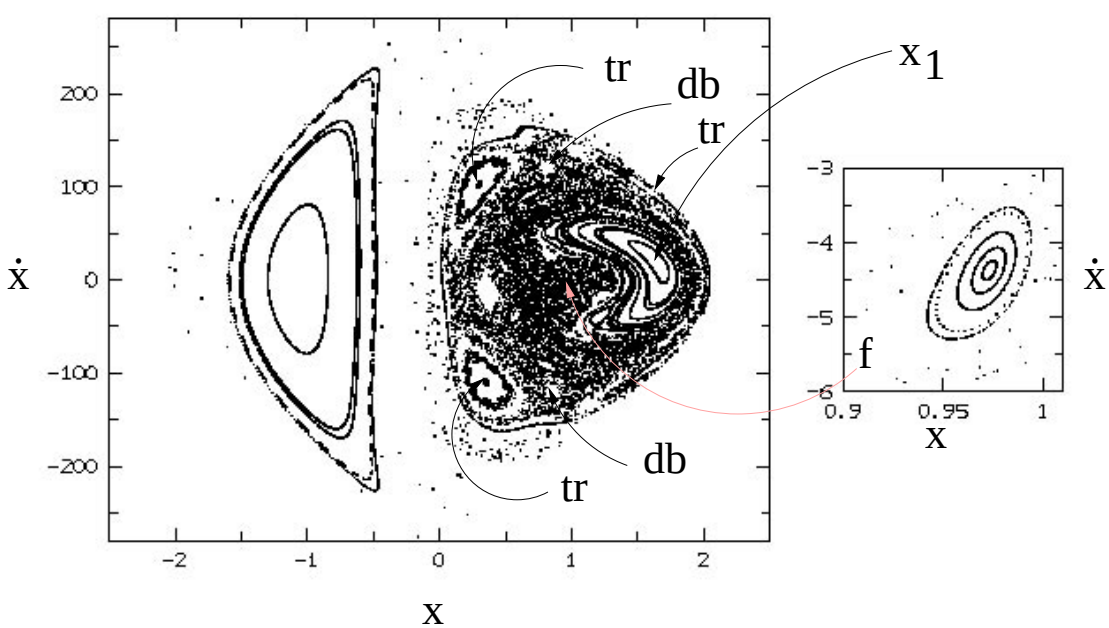

FIG. 21.—A Poincaré cross section at $E_J = -53{,}248.175$, i.e., in the UHR region in model "T." The initial conditions of the main periodic orbits are marked with the names of the families to which they belong.

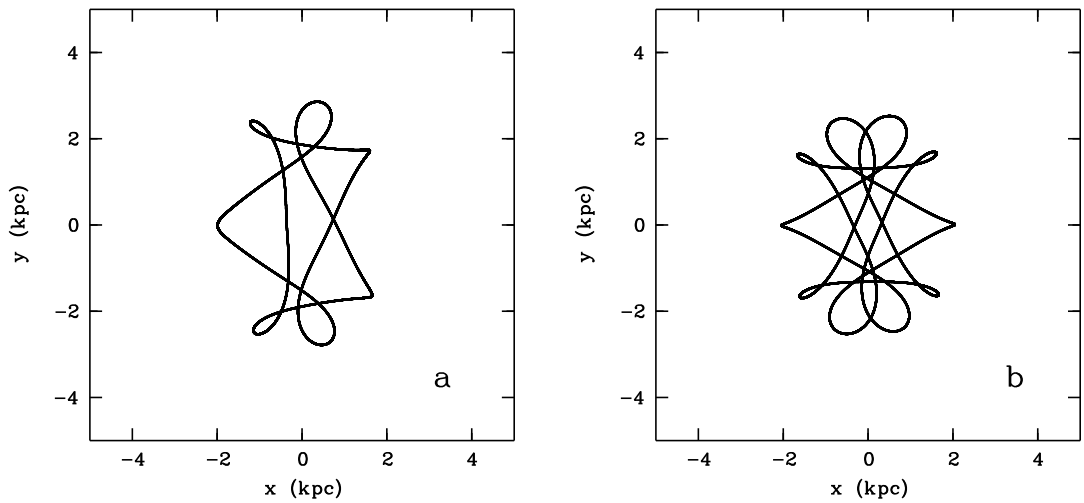

FIG. 22.—Stable periodic orbits of higher multiplicity at the UHR region in model "T." In (*a*) we give the double periodic orbit db and in (*b*) the triple periodic orbit tr.

the shape of the orbits at the apocenters is characterized by a boxy structure. This is formed either by "*f* type" rather straight parts (small sides of the rectangles) or by displaced loops of "x_1 type." A typical example is given in Figure 23*a*. The initial conditions for this orbit are $(x, \dot{x}) = (1.14, 86)$, i.e., far from the *f* periodic orbit, for which $(x_0, \dot{x}_0) = (0.97308883, -4.3670396)$. This and other similar examples clearly show that nonperiodic orbits with initial conditions at the chaotic region surrounding the periodic orbit *f* may strongly enhance the rectangular structure. The initial conditions for the orbit in Figure 23*b* are $(x, \dot{x}) = (0.7, 9.6)$.

We integrated several chaotic orbits for about 50 orbital periods of the x_1 or *f* orbit at the same E_J and saw that they still support the rectangular-like structure of the bar. In Figure 24 we give three such examples with initial conditions in the chaotic region. In (*a*) we again start relatively close to *f*, in (*b*) we have $(x, \dot{x}) = (0.90, -43)$, and in (*c*) $(x, \dot{x}) = (1, 90)$. Introducing a 400×400 Cartesian grid and integrating with equal time steps, we create an image of each orbit counting the number of points at each grid cell. Larger intensities (i.e., lighter parts on the figure) correspond to positions where the orbit passed more times than in the darker areas. In this way we have a crude estimation of the structures this orbit will support by locally enhancing the density of the bar. This can be better seen by applying a smoothing filter on the images. This is given in Figures 24*d* and 24*e* for Figures 24*a* and 24*b*, respectively. In all cases, a kind of rectangular shape is present. This is clear in Figures 24*a* and 24*c* and to a lesser extent in Figure 24*b*. For the orbit in Figure 24*c*, we give the contour of the space filled by the orbit, and we indicate by arrows the "straight segments" (*top*) that contribute in making the barrel-shaped contour with the flat small edges (*bottom*) (Fig. 24*f*). We note that the longer the area covered along the major axis of the bar, the more "*f* shaped" is the orbit. Athanassoula (1991, 1996) has already discussed the role of these orbits in forming the rectangular-like isophotes at the ends of bars. Furthermore, Pfenniger 1984b discussed chaotic orbits that could support structures, while their role in constructing self-consistent models of barred galaxies has recently been put forward by Kaufmann & Contopoulos (1996).

The general orbital behavior at the declining part of the x_1 characteristic is different from what we have seen for

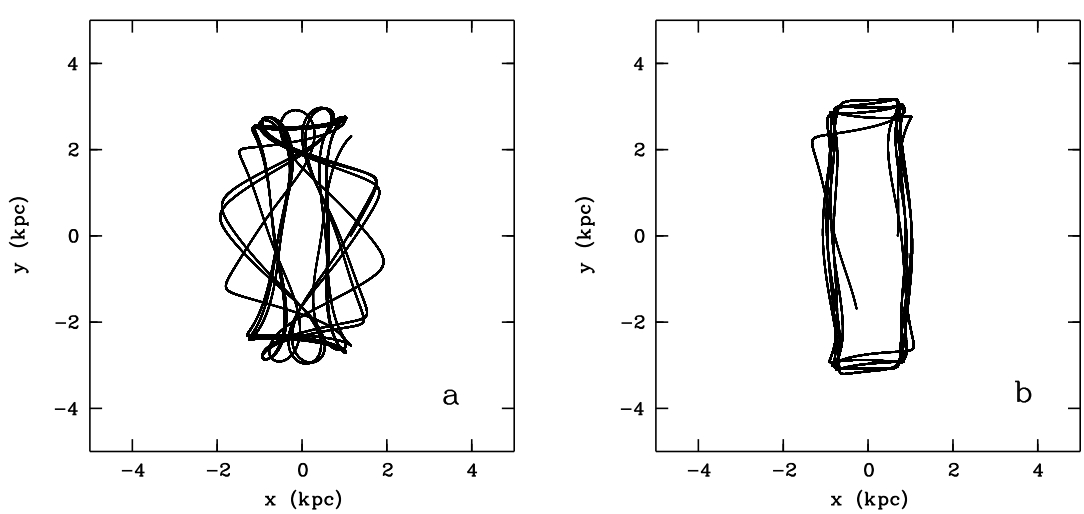

FIG. 23.—Nonperiodic orbits at the UHR region of model "T"

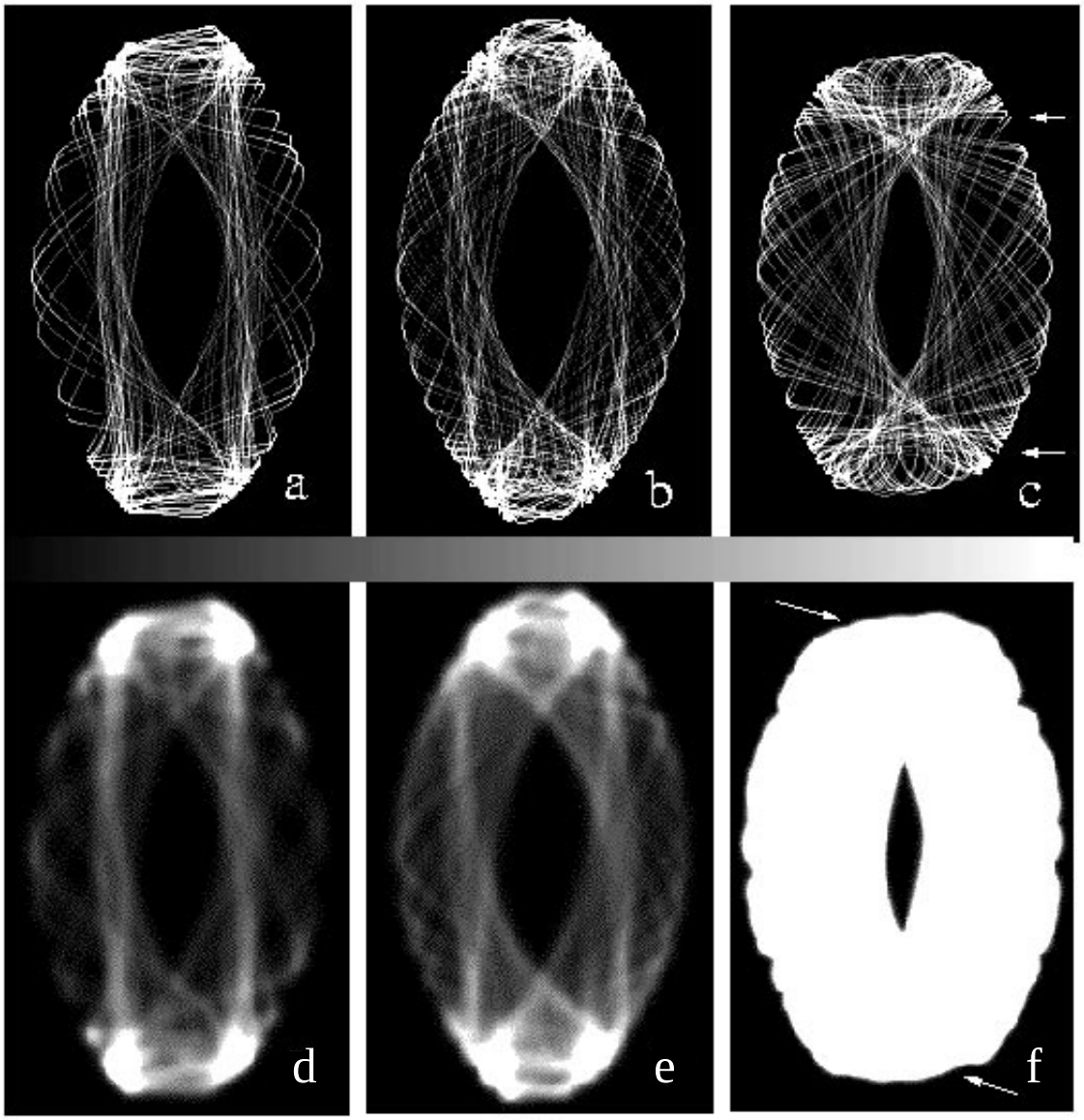

FIG. 24.—Images of orbits, with initial conditions in the chaotic region of Fig. 21, integrated for about 50 orbital periods of the x_1 or f orbit at the same E_J value. All of them support flat structures close to the end of the bar.

$E_J = -53{,}248.175$. Family x_1 is stable, but, as already mentioned, its orbits do not support the final extent of the bar toward corotation. The Poincaré surface of section for $E_J = -49{,}439.11$ is given in Figure 25*c*. The area occupied by the stable x_1 can be seen in the right central part. Quasi-periodic orbits follow the shape of the diamonds. These orbits could support structures across rather than along the bar (Fig. 25*b*). On the other hand, if we start integrating direct orbits starting from the nearby chaotic sea (between the area occupied by x_1 and the retrograde family at the center left-hand side in the Poincaré section), we observe that very soon the particles depart from the central region and then populate the areas to the left-hand and right-hand side of the Poincaré section. Thus, a test particle will not orbit for a long time along the bar (Fig. 25*a*) but will escape to larger radii, orbiting after that at the corotation region. The main conclusion is that neither quasi-periodic nor chaotic orbits beyond the distance of the 4:1 resonance influence the extent and shape of the bar in the QFG potential.

5.5. *Variation of* Ω_b

The corotation radius proposed by QFG for NGC 4314 is $70'' \pm 10''$. In our study we examined several "C"-type and "T"-type models with values of Ω_b giving a corotation radius in this range. In all cases we found basically the same orbital behavior as presented in the previous sections, with the resonant radii scaled according to the chosen Ω_b value. At the 4:1 resonance region, however, there is a difference between faster and slower rotating bars. The difference consists in the relative location [i.e., on the characteristic (E_J, x) diagrams] of the families x_1 and f, and of the families of orbits trapped around the Lagrangian points. We call these latter families "l" families. For fast rotating bars, like the cases we examined until now, their characteristics can be found at larger E_J's than those corresponding to the 4:1 region of the model. On the other hand, for $\Omega_b \lesssim 41$ km s^{-1} kpc^{-1}, parts of the characteristics of these families can be found close to the region where the x_1 characteristic declines with increasing E_J. They contain both stable and

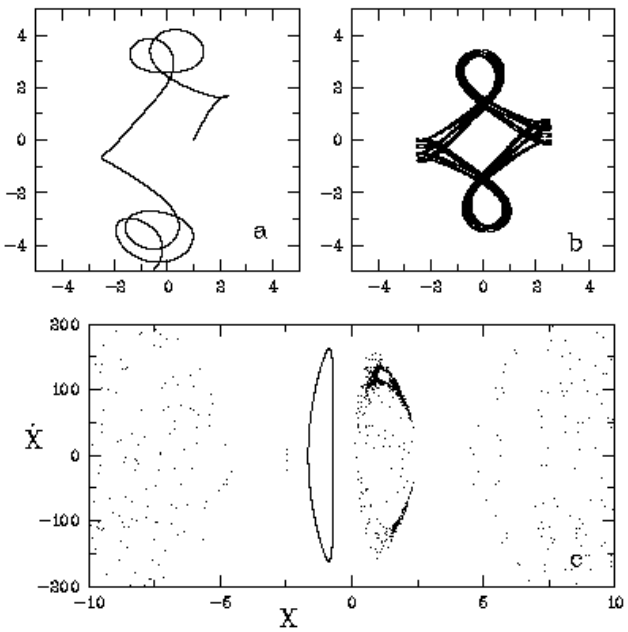

FIG. 25.—Nonperiodic orbits and a Poincaré section for $E_J = -49{,}439.110$.

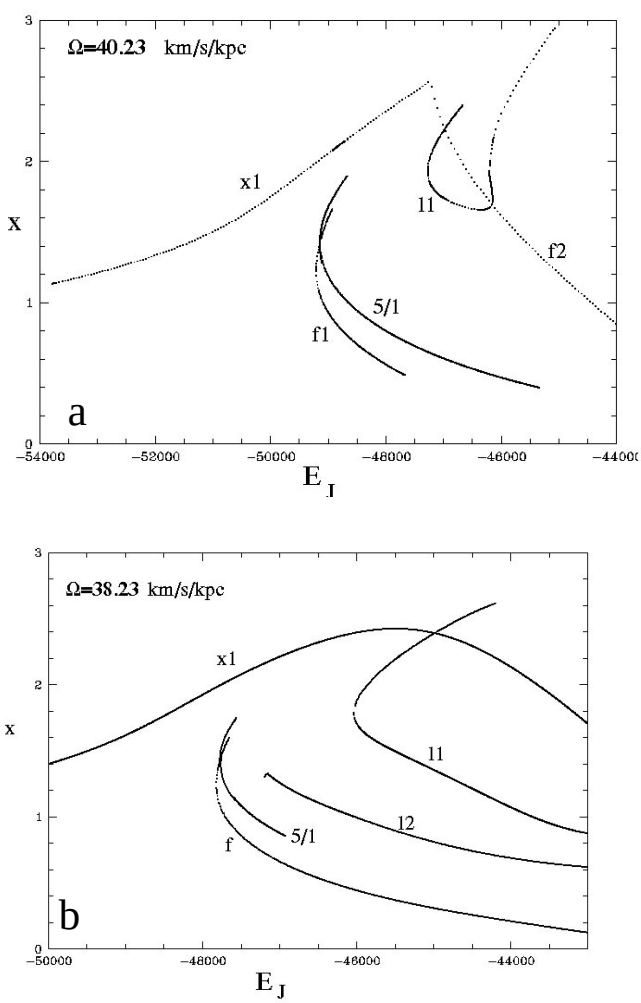

FIG. 26.—(E_J, x) diagrams of slow rotating bars. In (*a*) we give a "C" model with $\Omega_b = 40.23$ km s^{-1} kpc^{-1} and in (*b*) a "T" model rotating with $\Omega_b = 38.23$ km s^{-1} kpc^{-1}.

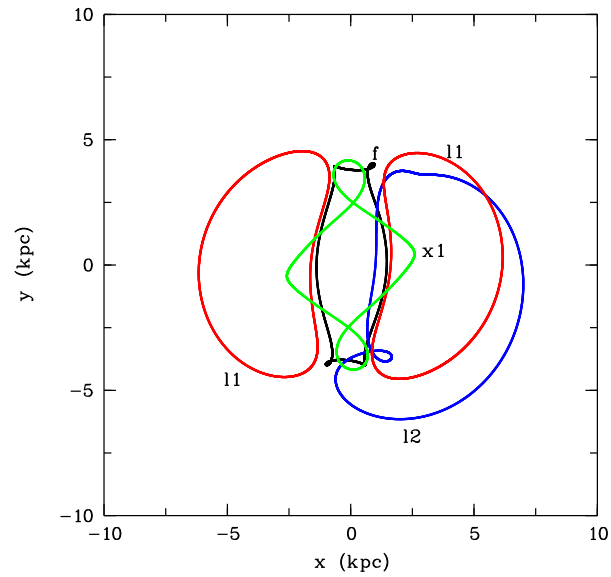

FIG. 27.—Orbits of the families encountered in the slow rotating model "T." The orbits are labeled according to the family to which they belong.

unstable parts. In Figure 26 we present two such cases, namely, a model of type "C" with $\Omega_b = 40.23$ km s^{-1} kpc^{-1} (Fig. 26*a*) and a "T" model with $\Omega_b = 38.23$ km s^{-1} kpc^{-1} (Fig. 26*b*). In this "T" model, corotation is located at 4 kpc (80″). Both stable and unstable parts are plotted with a continuous line on these diagrams. In Figure 26*a* the part of the branch of family l_1 to the left of f_2 is stable over a larger region than the stable part of f_1. In the case of Figure 26*b*, l_1 and l_2 have stable parts of about the same width as family *f*. Representatives of the families found in the "T" model having stable parts at the 4:1 resonance region and beyond are given in Figure 27. Obviously the orbits trapped around the Lagrangian points make test particles traverse both the bar and the outer disk region. Chaotic orbits, having $E_J \gtrsim -47{,}300$ and initial conditions close to the periodic orbits supporting the bar, typically follow for a few revolutions the rectangular- or diamond-shaped orbits and then cross corotation and follow *l*-type orbits for some time. This relation between the two types of 4:1 orbits and the *l* families has been also observed in *N*-body models, even in the case of a perturbed bar (Sundin 1993; Sundin et al. 1993). Thus, in the slowly rotating bar case many nonperiodic orbits with initial conditions below the x_1 curve and at the same time before, but close to, its declining part in the (E_J, x) diagram follow the *l* families. The *l* orbits, however, do not affect the orbital behavior at the region where the rectangular orbits are stable.

6. CONCLUSIONS AND DISCUSSION

We have examined the stability of the principal families of simple periodic orbits in a potential calculated by QFG directly from near-infrared observations of NGC 4314. The general conclusion of our paper is that the existing families of periodic orbits, their stability, and the general orbital behavior support, to a large extent, the observed morphology of the galaxy. This argues that the QFG potential is a good approximation of the potential of NGC 4314 in the plane of the disk. Furthermore, the orbital structure in the model is in agreement with the assumption of a bar rotating

as fast as to put the end of the bar inside but close to corotation. Further results can be summarized as follows:

1. The main structure in NGC 4314 is, of course, the bar. The orbits of the x_1 family are its main building blocks. Bifurcating families affect the dynamics of the system locally, namely, close to the n:1 resonance where they are generated. Away from their birth places, they are mainly unstable.

2. In the innermost regions of both models, i.e., for $r \lesssim$ 300 pc, we find families with both stable and unstable orbits. The orbital behavior encountered in this area is given with reservation because of the unrealistic definition of the potential in the center and the lack of the bulge component. In model "C" they are introduced as a continuation of the x_1 family, while in model "T" they are separate families. The ellipticity and orientation of their orbits vary along the characteristic curves, the former being particularly clear for family $x_{2,\,3}$ and the latter for family o_1. Thus, both near-circular and elongated orbits can be found in the innermost parts, i.e., in the region of the 1:1 and 2:1 resonances. It is interesting to note that the 2:1 resonance region corresponds to the region where a nuclear ring is observed. This coincidence, together with the fact that the potential is not accurate in this region, suggests that the ring might be a strong feature of the disk, the existence of which is not affected by the presence of a separate bulge component. To check this possibility and to see to what extent the exact form of the potential influences the stability and shape of the orbits in the inner parts, one should calculate orbits in potentials that are somewhat different in the innermost regions. In these new potentials it would be also necessary to examine the gaseous response in this area, since the ring is mainly a gaseous feature.

3. The role of orbits that are asymmetric with respect to the bar minor axis is important. At the 3:1 resonance region we have seen that the stable bifurcating families are the asymmetric ones. It is well worth noting that we find a preference for stable motion in this area. This is clearly seen in models of type "T," where the shape of the bifurcated family t_2, which is initially unstable, changes to t_1-type orbits in its stable part. The stable orbits in all cases are those with one side roughly parallel to the bar's minor axis. As already suggested by Athanassoula (1996), nonperiodic orbits around them could enhance the rectangularity of the bar. We have verified this by integrating several nonperiodic orbits in the 3:1 region. However, the extent of these orbits along the major axis of the bar does not exceed 2.5 kpc, so they do not contribute to the boxiness of the outer rectangular isophotes. Another asymmetric family found in the "C" models is f_2, which corresponds to the declining part of the x_1 family in the "T" models. These families introduce inclined diamond-like orbits close to corotation. These are in general the simple periodic orbits found closest to corotation. To put the whole matter in a nutshell, these asymmetric orbits, whose role is almost neglected in previous studies of barred potentials, provide the most important bifurcated families at the 3:1 resonance region, as well as just beyond the 4:1 resonance.

4. Although rather detailed, the information obtained from our orbital calculations does not provide any clear-cut solution to the existence of the outer boxy isophotes. The K′ image in QFG shows that the boxy isophotes inside corotation cover a radial distance along the bar major axis of $\approx 4''.6$, i.e., ≈ 230 pc. Furthermore, the northern side is more boxy than the southern one. The height difference between the shortest and the longest projections on the y-axis of the stable rectangular-like orbits found in the 4:1 resonance region of model "T" covers this radial extent of 230 pc. On the other hand, the phase space area occupied by the f and the 5:1 families is tiny. Yet, as argued initially by Athanassoula (1991, 1996), their effect may be enhanced by the behavior of neighboring orbits. As we have seen, if one chooses initial conditions close to but outside the area covered by the invariant curves of the periodic orbits, a chaotic orbit can stay close to the periodic one for several orbital periods. In this case its contribution to the density response will be similar to the contribution of a nonperiodic orbit trapped around the periodic one. In other words, chaotic orbits could support the rectangular structures for significant lengths of time. We have indeed, in all cases we have examined, found that chaotic orbits have major "horizontal" sections, almost parallel to the bar's minor axis and close to their apocenters. Another phenomenon, which seems to contribute even more to the formation of the small sides of the boxes, is the wobbling of the orbits trapped around the diamond-like x_1 orbits with loops, during which they fill an area with nearly straight parts at the two ends of the bar. To summarize, in a "T" model orbits in nonperiodic or chaotic motion at the 4:1 region, as well as further out, may occupy regions whose outline could explain the rectangular-like isophotes in this region. All the above suggest that the boxy isophotes are not directly related to a single family of periodic orbits but are a collective phenomenon reflecting the structure of phase space and the encountered orbital behavior at the 4:1 resonance region.

5. The extent of the bar is limited by the morphological evolution of the x_1 family. Beyond the 4:1 resonance the x_1 characteristic in the (E_J, x) diagrams declines with increasing energy (model "T") or becomes unstable, bifurcating a f_2 family (model "C"). This reflects the change of shape of its orbits. Beyond the UHR region family x_1 becomes strongly asymmetric. Stable orbits *do not help the bar extend toward corotation* because they shrink along the bar major axis and increase their loops as well as their projections on the minor axis. Thus, the longest stable periodic orbits are found at the 4:1 resonance region and are those that will mostly determine the outer structure of the bar. Quasi-periodic orbits reproduce this behavior, while chaotic orbits populate the corotation region and do not contribute to the bar density. This evolution of the shape of the x_1 family and its association with the termination of the bar has not been pointed out in other studies, probably because the role of the "asymmetric" orbits in barred potentials has been so far underestimated.

6. Our calculations show that "C"-type models are a reasonable approximation of the total potential. Although introduced in different ways, all important families have been found in the same region in both models. Nevertheless, "C" models fail to reproduce the twisting of the outer x_1 orbits roughly beyond the area of the 3:1 resonance. In "T" models all orbits have an initial $\dot{x} \neq 0$ component. The twisting becomes obvious for those orbits that are considerably peaked. This evolution of the x_1 orbits, in combination with the strongly "asymmetric" orbits beyond the UHR region, is responsible for the observed twisting of the outer isophotes in rectified images of several barred galaxies like NGC 1365, NGC 3953, and so forth. This reproduces rather

well the twist in the isophotes and argues that the sine terms are not negligible for the dynamics of many barred galaxies.

7. The range of Ω_b given by QFG corresponds to the rotation frequency of the bar in NGC 4314. From orbital studies alone it is difficult to decide if the lower or upper limit is closer to reality. However, we should remark that the slower rotating bars, which put corotation closer to the 80″ limit, give more space between the boxy isophotes and the end of the bar in the galaxy. The important role of the *l* families in these models may enhance the long sides of the boxes. Since we believe that the structure of the end of the boxes is determined by the orbital behavior at the UHR (for E_J values just before the *l* families appear in the system), it could be possible that orbits trapped around the Lagrangian points contribute to the rectangularity of the bar. In such a case a rather slower rotating bar would be preferable.

8. Finally, we find good agreement between the orbital behavior in the QFG potential and results of *N*-body simulations found in the literature. The close relation of the orbits we find in the 4:1 region and the orbits belonging to the *l* families is also present in the orbits found in the *N*-body simulations by Sundin et al. (1993; their Figs. 11*h*, 11*k*, and 11*l*). Interesting similarities are also found in the 3:1 families. The 3:1 type orbit given in Figure 11*j* of Sundin et al. (1993) stays for a long time close to an orbit resembling our stable orbit in Figure 19*e*. On the other hand, the 3:1 orbit in their Figure 11*f* deviates fast from an orbit resembling our unstable 3:1 periodic orbit in Figure 19*d*. Agreement with typical *N*-body orbits in barred galaxy simulations found by Sparke & Sellwood (1987; e.g., their Fig. 10) should also be mentioned.

We have benefited from discussions with Albert Bosma and Kevin Prendergast. P. A. P. also acknowledges fruitful correspondence with Dave Kaufmann. We would like to thank IDRIS (Institut du Développement et des Ressources en Informatique Scientifique, Orsay, France) for the allocation of computer time.

REFERENCES

Athanassoula, E. 1991, in Dynamics of Disc Galaxies, ed. B. Sundelius (Göteborg: Univ. Göteborg), 149
———. 1992a, MNRAS, 259, 328
———. 1992b, MNRAS, 259, 348
———. 1996, in Spiral Galaxies in the Near-IR, ed. D. Minniti (Berlin: Springer), 147
Athanassoula, E., Bienaymè, O., Martinet, L., & Pfenniger, D. 1983, A&A, 127, 349
Athanassoula, E., Morin, S., Wozniak, H., Puy, D., Pierce, M., Lombard, J., & Bosma, A. 1990, MNRAS, 245, 130
Ball, R. 1992, ApJ, 395, 418
Barbanis B., & Woltjer L. 1967, ApJ, 150, 461
Benedict, G. F., Higdon, J. L., Tollestrup, E. V., Hahn, J. M., & Harvey, P. M. 1992, AJ, 103, 757
Benedict, G. F., et al. 1993, AJ, 105, 1369
Block, D. L., Bertin, G., Stockton, A., Grosbøl, P., Moorwood, A. F. M., & Peletier, R. F. 1994, A&A, 288, 365
Contopoulos, G. 1983a, Cel. Mech., 31,193
———. 1983b, ApJ, 275, 511
———. 1988, A&A, 201, 44
Contopoulos, G., & Grosbøl, P. 1986, A&A, 155, 11
———. 1989, A&A Rev., 1, 261
Contopoulos, G., & Papayannopoulos, Th. 1980, A&A, 92, 33 P. O. Lindblad(eds.) - Springer-Verlag
de Vaucouleurs, G., de Vaucouleurs, A., Corwin, H. G., Jr., Buta, R. J., Paturel, G., & Furgue, P. 1991, Third Reference Catalogue of Bright Galaxies (New York: Springer)
Friedli, D., Wozniak, H., Rieke, M., Martinet, L., & Bratschi, P. 1996, A&A, in press
Frogel, J. A. 1988, ARA&A, 26, 51
Garcia-Baretto, J. A., Downes, D., Combes, F., Gerin, M., Magri, C., Carrasco, L., & Cruz-Gonzalez, I. 1991, A&A, 244, 257
Grosbøl, P. J. 1985, A&AS, 60, 261
Hénon, M. 1965, Ann. d'Astrophys., 28, 992
Kaufmann, D. E., & Contopoulos, G. 1996, A&A, 309, 381
Papayannopoulos, Th., & Petrou, M. 1983, A&A, 119, 21
Patsis, P. A., & Grosbøl, P. 1996, A&A, 315, 371
Pfenniger, D. 1984a, A&A, 134, 373
———. 1984b, A&A, 141, 171
Pfenniger, D., & Friedli, D. 1991, A&A, 252, 75
Quillen, A. C., Frogel, J. A., & González, R. A. 1994, ApJ, 437, 162 (QFG)
Quillen, A. C., Frogel, J. A., Kenney, J. D. P., Pogge, R. W., & DePoy, D. L. 1995a, ApJ, 441, 549
Quillen, A. C., Frogel, J. A., Kuchinski, L. E., & Terndrup, D. M. 1995b, AJ, 110, 156
Regan, M. W., Vogel, S. N., & Teuben, P. J. 1995, ApJ, 449, 576
Shaw, M., Axon, D., Probst, R., & Gatley, I. 1995, MNRAS, 274, 369
Sparke, L., & Sellwood, J. 1987, MNRAS, 225, 653
Sundin, M. 1993, Ph.D. thesis, Chalmers Univ., Göteborg
Sundin, M., Donner, K. J., & Sundelius, B. 1993, A&A, 208, 105